A&A 426, 855–865 (2004)
DOI: 10.1051/0004-6361:20035887

Astronomy & Astrophysics

Coordinated observation of local interstellar helium in the Heliosphere

EUVE observations of the helium glow: Interstellar and solar parameters

J. Vallerga[1], R. Lallement[2], M. Lemoine[3], F. Dalaudier[2], and D. McMullin[4]

[1] Space Science Laboratory, University of California, Berkeley, 94720-7450, USA
e-mail: jvv@ssl.berkley.edu
[2] Service d'Aéronomie du CNRS, 91371 Verrières-le-Buisson, France
[3] Institut Leprince-Ringuet, École Polytechnique, 91128 Palaiseau, France
[4] Space Sciences Center, University of Southern California, Los Angeles, CA 90089 Praxis, Inc., 2200 Mill Road, Alexandria, VA 22314, USA

Received 16 December 2003 / Accepted 2 March 2004

Abstract. We present new observations of the diffuse He I 58.4 nm background recorded in 1998 and 2000 by the Extreme Ultraviolet Explorer (EUVE). This emission is due to resonant scattering of the solar EUV radiation by interstellar and geocoronal helium. Depending on the geometry and relative velocity, a fraction of the interstellar helium glow can be absorbed by the line-of-sight geocoronal gas. The new results are combined with measurements obtained in 1992–93 and previously analyzed by Flynn et al. (1998). A kinetic model of the helium flow is now used to analyze the data and reproduce the absorption features due to geocoronal helium. This allows a precise determination of the interstellar flow bulk velocity vector. A model that includes both photoionization and electron impact ionization was fit to the data set. New constraints on the interstellar helium flow temperature and density, as well as on the solar 58.4 nm line width are obtained. The interstellar helium velocity vector parameters, $\lambda = 74.7 \pm 0.5°$, $\beta = -5.7 \pm 0.5°$, $V_{\rm He} = 24.5 \pm 2$ km s^{-1}, are found to be in good agreement with those derived from particle measurements. Using the solar He I 58.4 nm flux and photoionization rate proxies of McMullin et al. (2003), the neutral helium density and temperature derived from the Long Wavelength Spectrometer data is $n_{\rm He} = 0.013 \pm 0.003$ cm^{-3}, and $T_{\rm He} = 6500 \pm 2000°$ respectively, again in good agreement with particle data. However, the width of the downwind cone when scanned across the latitudnal direction tends to be fit better with higher He temperatures, which might indicated latitude anisotropies in the He ionization that we have not included in our models.
The solar He I 58.4 nm Doppler width, $\Delta w_{\rm D}$, is found to be =0.0074 nm, (or 38 ± 3 km s^{-1}) in 1992–1993, i.e. near solar maximum, and $\Delta w_{\rm D} = 0.0087$ nm (45 ± 3 km s^{-1}) in 1998, after solar minimum, in agreement with SOHO SUMER and CDS results, although again, the 1998 fits near solar minimum might suffer from latitudinal anisotropies.

Key words. interplanetary medium – ISM: kinematics and dynamics – ISM: atoms – Sun: UV radiation – palsmas

1. Introduction

The flow of interstellar helium atoms in the solar system has been observed by means of its resonant scattering of solar He I 58.44 nm radiation for three decades, but by a very limited number of experiments (Weller & Meier 1981; Dalaudier et al. 1984; Flynn et al. 1998). For a historical review see Lallement (2002). As opposed to neutral hydrogen, interstellar neutral helium is only weakly coupled to the charged particles, so it has the very useful property of being insensitive to the heliospheric interface, and therefore penetrates freely into the inner heliosphere. It is thus an important tracer of the conditions which prevail in the local interstellar cloud surrounding the Sun, and can be used as a reference for measuring the perturbations of neutral hydrogen at the heliospheric interface crossing, i.e. deceleration, heating and filtration (Lallement 1999; Costa et al. 1999).

The Extreme Ultraviolet Explorer satellite (EUVE, Bowyer & Malina 1991) had two instruments sensitive to 58.4 nm solar photons, both interplanetary and geocoronal. This radiation was the dominant background source through the life of the satellite (June 1992 to re-entry in January 2002). Therefore data exist for the interplanetary helium glow for the nine years of continuous night-time observations by EUVE. Most of these data were pointings towards celestial EUV point sources corresponding to arbitrary lines of sight through the interplanetary helium and provide single line of sight measurements contaminated by variable geocoronal backgrounds. Of more use are the short timescale scans across the sky undertaken in sky–survey mode where the background is relatively constant and easier to model and the signal flux shows more contrast due to its large scale angular structure.

EUVE data from the initial all–sky survey recorded in 1992–1993 were presented in Flynn et al. (1998, hereafter

referred to as FVDG). The results were analyzed with the help of a kinetic model for the density distribution, and an approximate analytical formula for the analysis of the geocoronal absorption. In the present work, a fully kinetic model is used, and ionization of helium by electron impact ionization is now included. Electron impact ionization differs from photoionization of helium in that it does not vary as r^{-2} (r is the distance to the Sun) and requires a numerical approach. The influence of electron impact ionization is weak for lines-of-sight outside 1 AU, but non negligible for anti-solar lines-of-sight in the downwind region. Finally, the knowledge of the four solar parameters, i.e. the solar He I 58.4 nm linewidth and irradiance, the photoionization rate, and the electron impact rate, has considerably progressed since the first observations in 1992−93, essentially due to SOHO spectrographs and coronographs, and these added constraints improve the derived helium parameters.

Since 1993, specially planned measurements of the helium glow were obtained with EUVE in 1997, 1998, 2000. These observations were designed to emphasize the contrast in the signal by choosing to point to strong features in the signal distribution, thus providing stronger constraints for the model parameters. We have used a set of data, carefully selected, such that all main interstellar and solar parameters can be derived nearly independently. Other data are found to be compatible with the resulting model parameters. The data used to constrain the model are: (i) the entire set of the EUVE Long Wavelength Spectrometer (LWS) data recorded between July 1992 and July 1993. These data are not significantly contaminated by geocoronal emission and represent a unique series of anti-solar measurements over a full year, at a high solar activity time. (ii) EUVE Scanner C (ScC) data recorded in February 1993; (iii) unpublished ScC data recorded in February 1998, i.e. at moderate solar activity. ScC data obtained in October 2000 are also compared with the model and shown to be compatible. The data and geometry are presented in detail in Sect. 2. The model is presented briefly in Sect. 3. We have checked that all data other than those presented here can be fitted to the same interstellar parameters and appropriate solar parameters, allowing for a reasonable level of geocoronal emission. Model adjustment to the entire set of EUVE data requires a sophisticated model of the geocoronal density distribution and will be the subject of future work.

We now detail the logical sequence of data-model adjustments we performed (results given in Sect. 4).

First, we revisit the 92−93 LWS anti-solar data and use the downwind data to derive the interstellar flow longitude. We then use the Feb. 15−16, 1993 scan and the geocoronal absorption signature to constrain the wind latitude. Next, we use both the new Feb. 15−16, 1998 scan and the Feb. 15−16, 1993 data, and the geocoronal absorption signature they both exhibit, to derive the interstellar flow velocity modulus. Using the parameters for the helium velocity vector derived above we model the 92−93 LWS data and derive constraints on the solar He I 58.4 nm linewidth from the upwind intensity pattern. We also use the Feb. 98 scan to derive a slightly stronger lower limit on the solar linewidth. If combined, these results allow us to constrain the solar He I 58.4 nm linewidth within a relatively narrow interval, thought the validity of this approach is questionable given that they were done at different phases of the solar cycle. Using the same data, now including the focusing cone region, we derive the flow temperature and its density, assuming the solar photo-ionisation rate and the solar He I 58.4 nm intensity are those derived by McMullin et al. (2003), and the electron impact rate as predicted by Lallement et al. (2003). Conversely we adopt the flow temperature and density measured by Ulysses-Gas (Witte et al. 2003) and derive the ionization rate and the solar intensity.

Adopting the derived set of parameters, we show the data-model comparison for the Oct. 2000 scans, and find a good agreement except for line-of-sight characterized by a local zenith angle exceeding about 80°. Finally, we discuss in Sect. 5 the parameters derived from the EUVE data and compare them with other determinations.

2. EUVE data

The EUVE spacecraft had four telescopes that fed seven science instruments, consisting of four photometric imaging systems and three spectrometers with overlapping spectral ranges. Three of the telescopes illuminated the three scanner detectors and the fourth was devoted to the deep survey and three spectrometer detectors. The three scanner telescopes were co-aligned with a boresigth oriented 90° from the deepsurvey/spectrometer telescope boresight. Details of the EUVE instrumentation are given by Bowyer & Malina (1991) and Sirk et al. (1997) and references therein.

Each of the three scanners had a ∼5° circular field of view divided into separate broad band filter quadrants. Scanners A and B had identical filter combinations and were sensitive to the range 7−29 nm and Scanner C was sensitive to the longer wavelengths (40−70 nm). In particular, the tin filter quadrants with passbands of 40−75 nm, were sensitive to the 58.4 nm emission. The long wavelength spectrometer (LWS) had a passband sensitive to both HeI 58.4 nm and HeII 30.4 nm. The LWS was an objective spectrometer designed for point sources and therefore did not have a slit. However, it did have a wire grid collimator with a ∼triangular field of view of $20' \times 2.1°$. Table 1 lists the effective area and solid angle of the instruments. The effective area values were based on ground calibrations traceable to standard photodiodes with absolute efficiencies good to 25%. The solid angles are based on the plate scale and vignetting functions determined from in-orbit pointings towards hot white dwarfs (Sirk et al. 1997). Repeated measurements of EUV sources detected no degradation of the sensitivity greater than 10% from 1992 to 1998 (Sirk et al. 1997; Vallerga et al. 1998). It must be pointed out, however, that calibrations of the total diffuse response (effective area times the effective solid angle) is fraught with assumptions of the uniformity and smoothness of the optics and detectors though only measured at a few locations with point sources. For a complete discussion of the data extraction techniques for the neutral helium observations, we refer the reader to FVDG.

In the standard survey mode, the EUVE scanners made 360° sweeps of the sky in a plane perpendicular to the anti-solar direction. The scan azimuth is defined as 0° when the scanners were pointed to the ecliptic north. The LWS observed

Table 1. EUVE Instrumentation.

Instrument	Passband, nm	Field of view	Ω, sr	A_{eff}[a] cm^2
Scanner C (ScC)	52–74	2.1°[b]	8.0×10^{-4}	0.43
Long Wavelength Spectrometer (LWS)	28–76	2.1°×20′	1.3×10^{-4}	0.18

[a] Effective area at 58.4 nm.
[b] Field of view is a quadrant of a 2.1° radius circular aperture.

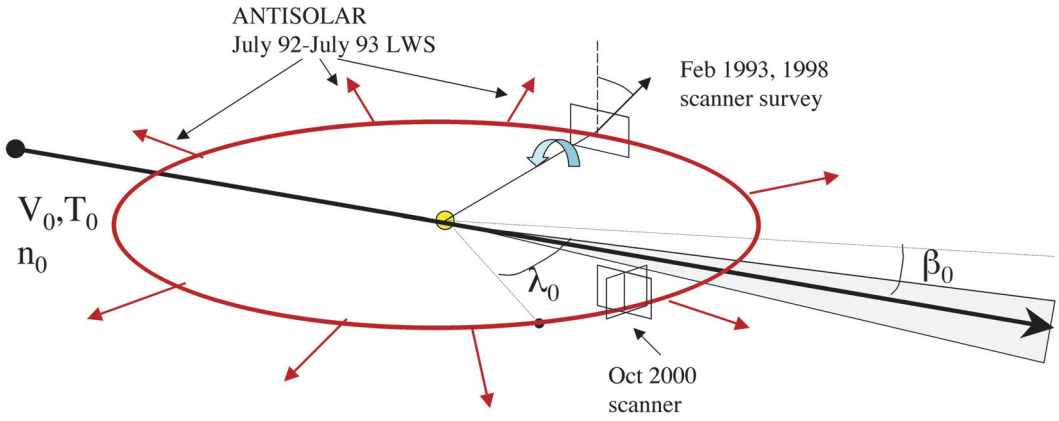

Fig. 1. The pointing geometry of the EUVE LWS and Scanner instruments with respect to the Earth's orbit and the interplanetary wind velocity vector (see text).

in the anti-solar direction down the Earth's shadow, therefore eliminating most of the single scattered background from the illuminated geocorona. Figure 1 shows the viewing geometry. In this survey mode, the satellite rotation rate was approximately 3 rotations per orbit or one 360° sweep per orbital nighttime. Depending on time of year and rotation direction and phase, the downwind He cone observed by the scanners could appear at any time during the scan. Preferably, the best orbits had the cone observed at orbital midnight, since the dusk and dawn 58.4 nm background increased exponentially as the terminators were approached. In all of our models of the scanner data, we fit the geocoronal background vs. scan angle as a constant plus a linear slope to account for a dusk/dawn asymmetry in scattered 58.4 nm plus two steeply increasing exponential terms at dawn and dusk to reflect the "bathtub" shape of the geocoronal background. The observations presented below for February 15–16, 1993 and 1998 are examples of the standard survey. They consist of the average of 7 and 10 orbits of nighttime scans respectively.

We attempted something different for the October, 2000 scans. First, we decreased the rotation rate such that we scanned only over 180° during orbital night, phased such that the helium cone was observed at approximately midnight. We performed 5 separate scans of 5 orbits each, different by the direction of the rotation vector such that the scan plane intersected the helium cone at 5 different radial distances from the sun. The rotation axis stayed in the ecliptic plane, but each set of scans were offset by ≈5° in longitude. The goal was to test our models on their dependence with respect to the distance to the Sun. The first observation started 19h UT, Oct. 17, 2000 and the fifth started at 9hUT, Oct. 19, 2000. Unfortunately, our detailed planning overlooked the local zenith angle of the line of sight, which dipped greater than 80 degrees from the zenith for small fractions of the orbit resulting in attenuated and sometimes enhanced flux due to atmospheric effects.

Though the geocorona dominates our background and complicates our analysis due to its variabiltiy in time and space, there was one geocoronal effect that worked to our advantage: the geocorna's neutral helium absorption of the 58.4 nm interplanetary flux. Because of the lower effective temperature of the neutral helium geocorona and the high absorbing cross section (≳10 optical depths), the Earth's atmosphere acts like a helium absorption cell with a spectral width comparable to that of the interplanetary helium at a temperature of ≈6500 K (see FVDG). The measured flux has a very strong dependence on the relative velocity of the Earth and the helium being observed in the line-of-sight. We have used this effect to constrain the latitude component of the flow velocity vector as well as its modulus (Sect. 4).

The LWS was less sensitive to diffuse 58.4 nm than ScC (1.8 cts s^{-1} R^{-1} vs. 63 cts s^{-1} R^{-1} respectively), but during the 92–93 all sky survey, it observed only down the Earth's shadow cone where the geocoronal background was minimized. For each 15 orbits of the survey, which commenced on day of year 206, 1992, we generated a single flux value, correcting for particle and HeII 30.4 nm background by scaling from the count rates in the Short and Medium Wavelength spectrometers (see FVDG). Data that were contaminated by the SAA and geomagnetic storms were excluded. This data set is orthogonal to the scanner data set, as it samples the longitudnal distribution of the neutral helium 58.4 nm flux at a constant ecliptic latitude (=0° see Fig. 1). Because the timescale of this

ecliptic survey is on the order of a year rather than hours to days, we must correct for the illuminating solar flux variation, which we scale using the Mg II proxy of the 58.4 nm flux (McMullin et al. 2004). Residual variability still exists in our data on the timescale of ∼days, which we attribute to inaccuracy of the proxy model to solar transients and solar linewidth variations as well as inaccurate background subtraction of particle flux using other detectors as reference.

3. Modeling

Because neutral helium is not perturbed at the entrance in the heliosphere, it is possible to model the glow data with the help of a simple one-fluid, mono-temperature model (the so-called classical "hot model", see e.g. Dalaudier et al. 1984). The gas is assumed to have a Maxwellian distribution far from the Sun, and thus characterized by its density $n_{\rm He}$, bulk velocity $v_{\rm He}$ and temperature $T_{\rm He}$. Individual atoms are followed along their trajectories from infinity to any location in the solar system, and at each solar distance, r, along these trajectories are computed the losses due to photoionization and collisional electron ionization at rates $\nu_{\rm Ph}(r)$ and $\nu_{\rm El}(r)$ respectively. The radial velocities at any point P of all test atoms reaching P are computed and used along with their contributions to the local density. The solar He I line has a limited Doppler width $\Delta w_{\rm D}$, of the order of the helium atomic velocities. Because an individual atom with radial velocity $w(r)$ scatters resonantly only those solar photons which have wavelengths λ that equal $\lambda_0(1. - w(r)c^{-1})$, the diffuse intensity is proportional to $I_0 \exp(-((\lambda - \lambda_0)/\Delta\lambda_{\rm D})^2) = I_0 \exp(-(w(r)/\Delta w_{\rm D})^2)$ if I_0 is the solar 58.4 nm intensity at line center.

A version of the model adds the computation of the velocity vector of any atom reaching point P, which is necessary to calculate the local contribution from P to the line-of-sight integrated emission line profile. This emission line profile is required to model the absorption of the interplanetary emission by the cold geocorona, in which the EUVE instruments reside. In what follows the geocorona is assumed to be a volume of gas at rest with the earth and at a uniform temperature $T_{\rm g}$ (Doppler width $\Delta\lambda_{\rm g}$). Along a given line-of-sight (LOS), terrestrial atoms constitute a column-density $N_{\rm g}$ and the interplanetary profile $I(\lambda)$ has to be convolved by the transmission $\exp(-\tau \exp(-((\lambda - \lambda_0 - \lambda_{\rm g})/\Delta\lambda_{\rm g})^2))$, where $\lambda_{\rm g}$ is the wavelength Doppler shift due to the earth's velocity along the LOS and the geocoronal optical depth $\tau = \sigma N_{\rm g}$ is the product of the column density by the resonance cross-section σ.

The 58.4 nm line-integrated solar intensity appropriate to the observation dates is taken from the proxy built by McMullin et al. (2004), i.e. $2.1 \pm 0.2 \times 10^9$ ph cm^{-2} s^{-1} for the Feb. 15−16, 1993 data, and $1.7 \pm 0.2 \times 10^9$ ph cm^{-2} s^{-1} for the Feb. 15−16, 1998. It is important to note that the flux at line center for a given total intensity is a function of the Doppler width. Since atoms do not scatter with the same efficiency a broad or a narrow line, this means that the diffuse intensity is a function of both the total line-integrated flux and the linewidth.

The photoionization rate at 1 AU is also taken from the proxy built by McMullin et al (2005), i.e. $1.0 \pm 0.15 \times 10^{-7}$ s^{-1} for the Feb. 15, 1993 data, and about $0.9 \pm 0.1 \times 10^{-7}$ ph cm^{-2} s^{-1} for Feb. 16, 1998.

The ionization by electron impact is included in the model (Rucinski & Fahr 1989; Lallement et al. 2004). The ionization rate is solar cycle dependent and SOHO-UVCS data suggest that it varies by a factor of about 3.5 with the solar activity. According to this analysis, the Feb. 93 data require a rate about twice the solar minimum rate of Rucinski et al. (1988), while the Feb. 98 data require a rate about the same as at the solar minimum value.

The solar linewidth has been measured by both CDS and SUMER on board the SOHO satellite. Both instruments have produced spectra of small regions on the solar disk. The SUMER instrument has also measured the disk-integrated emission linewidth, following a method devised by Bertaux in 1996. The SUMER average Doppler linewidth is found approximately constant throughout the solar cycle rise and to be $\Delta w_{\rm D} = 36.5 \pm 1.7$ km s^{-1} (see McMullin et al. 2004, for the SUMER results). This is in good agreement with the SUMER full disk values of $\Delta w_{\rm D} = 38 \pm 3$ km s^{-1} in November 96 and $\Delta w_{\rm D} = 42 \pm 3$ km s^{-1} in November 2000 (Lemaire 2003). This is an enormous advantage to be able to rely on these SOHO measurements. Earlier analyses have somewhat suffered from uncertainties on this parameter (see Lallement et al. 2004b, this issue).

4. Analysis

4.1. Helium flow longitude

Figure 2 shows the intensities measured with the LWS in the anti-solar direction from July 1992, to July 1993, as a function of the earth ecliptic longitude. Data have been corrected for solar intensity variations in a way which will be discussed in Sect. 5. The focusing cone is conspicuous and thanks to the observing strategy it is easy to derive the wind axis longitude, which is the earth longitude corresponding to the maximum intensity, independently of any other parameter. From a simple Gaussian or other symmetric model, we derive $\lambda_w = 74.7 \pm 0.5°$.

Note that the preliminary analysis by FVDG led to a slightly different value. The reason for the discrepancy was traced to a small but significant error in the calculation of the Earth's ephemerids. This newly determined flow longitude is in excellent agreement with the direction derived from previous UV measurements (e.g; Prognoz analysis gave $\lambda_w = 74.5 \pm 1°$, Dalaudier et al. 1984) and from in situ data (Witte et al. 2004).

4.2. Helium flow latitude

The flow latitude is not as straightforward to derive as the longitude, and its determination from intensities and particle fluxes is somewhat model dependent. In the past some discrepancies between the previous glow and particle measurements have been noted. A good way to measure the latitude is to use the geocoronal absorption features. As described in FVDG, the geocoronal neutral helium acts as an absorption cell, and its imprints depend on the relative velocity vector between the earth and the helium flow. The latitude has been already derived

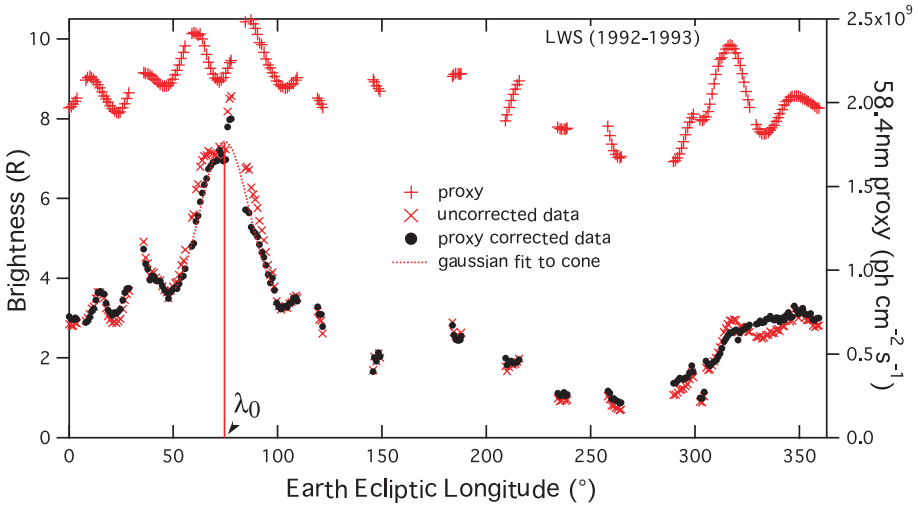

Fig. 2. Determination of the He wind longitude. Antisolar data corrected for solar line intensity fluctuations are fitted by a Gaussian profile in the ecliptic longitude range 50−100 degrees.

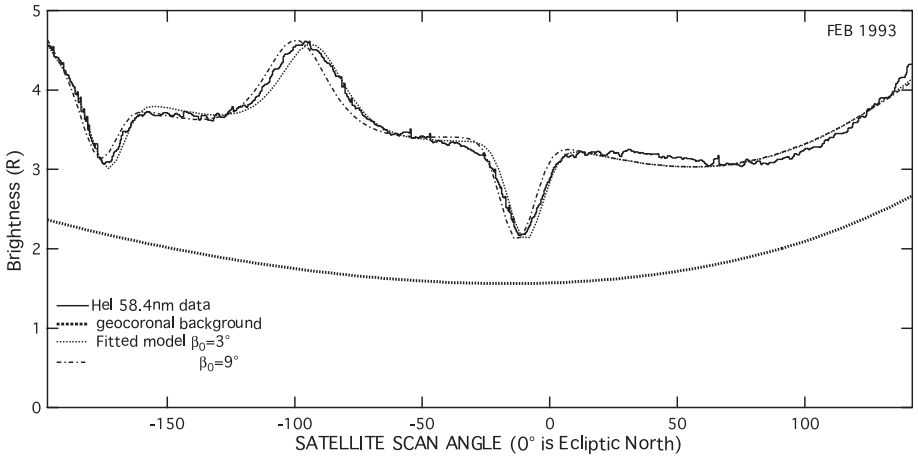

Fig. 3. He wind latitude determination. The geocoronal absorption features and the cone apparent direction depend on β_0. Here the Feb. 15, 1993 scan is used to measure β.

by FVDG using the Scanner data of March, 1993. However, because we use a kinetic model with self-consistent line profiles and intensities, it is useful to repeat this analysis. We show here the results on the Feb. 15, 1993 scan (Fig. 3). The derived latitude is $\beta = -5.7 \pm 0.5°$, in good agreement with Dalaudier et al. 1984, and compatible with the new results of the particle data (Witte et al. 2004)

4.3. Flow velocity modulus

As we have seen, kinematical parameters are best constrained from geocoronal absorption features, and this is particularly true for the velocity modulus. During a angular scan such as the lateral scans performed with the Scanner C, the maximal geocoronal absorption occurs when the earth absorption is at the center of the emission profile. For this null Doppler shift direction, the bulk flow is perpendicular to the LOS. FVDG used the scanner data of March 1993 and the location of maximum absorption, and found $v_{\rm He} = 26.4 \pm 1.6$ km s^{-1}. However, this derivation was based on an approximate model, and the influence of the slope of the additional geocoronal emission was not taken into account.

We used our kinetic model and the new, high signal to noise Feb. 1998 data to reinvestigate this point. While the absolute location of each absorption feature depends mostly on two parameters, i.e. the latitude of the flow and the bulk velocity, the angle difference, $\Delta\phi$, between the two absorption features only depends on the bulk velocity. If trajectories were straight lines and in the absence of extinction, the two absorption features would both be perpendicular to the bulk flow and at $\Delta\phi = 180°$ from each other. Due to the gravitational focusing (and in a minor way to fast particle selection effects), the angle is different, but the bending of the trajectories depends essentially on the initial velocity. The smaller the velocity, the larger the bending of the helium trajectories, and as a consequence the smaller the angle between the two directions with maximum absorption. For a series of models corresponding to different bulk velocities the best fit combination of the model and a smoothly varying geocoronal emission has been adjusted to the data. For each model the angle between the two LOS with maximal

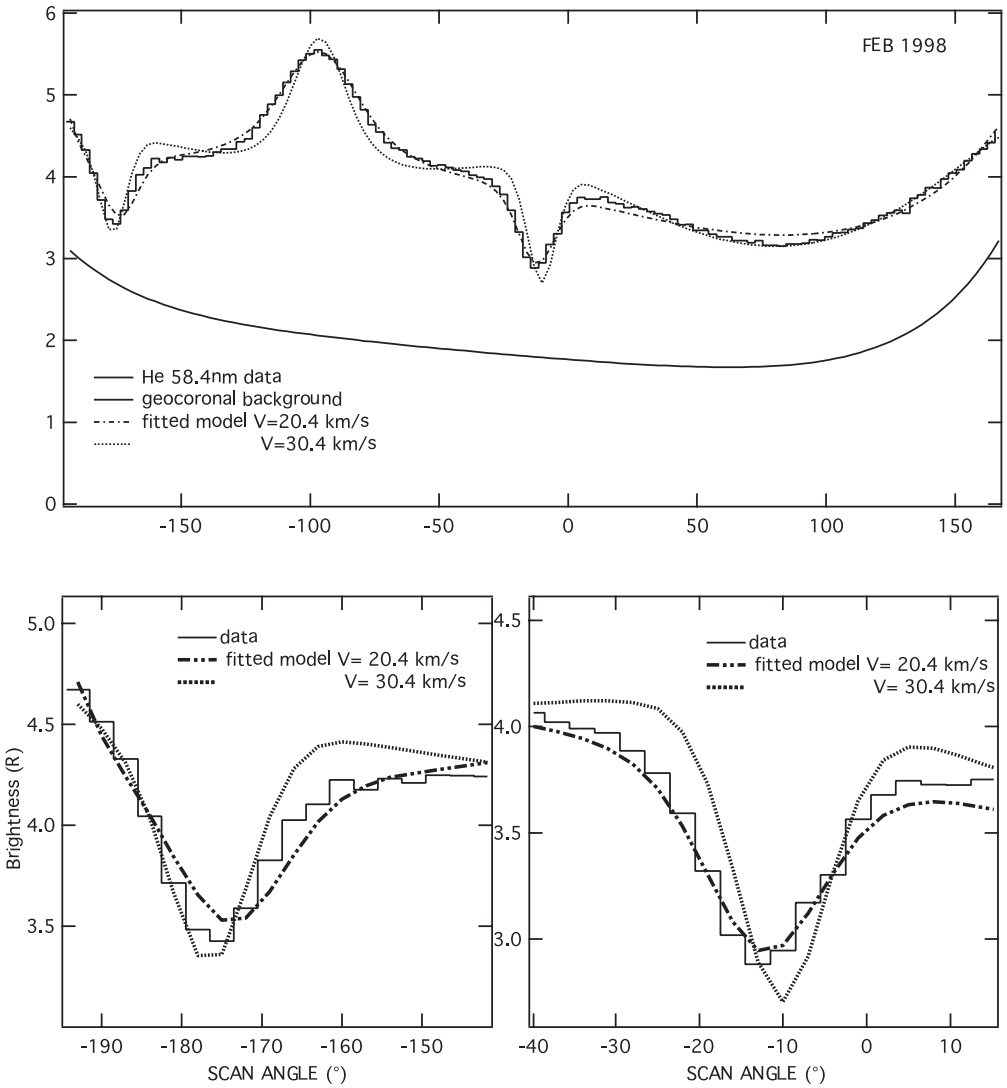

Fig. 4. Determination of the He flow velocity modulus with the Feb. 98 data.

geocoronal absorption is calculated, providing a relationship between the angle $\Delta\phi$ and the velocity modulus $v_{\rm He}$. The bulk velocity is then determined by interpolation using the measured angle $\Delta\phi$. With this method, biases linked to the geocoronal emission and absorption shape and to the flow latitude are avoided.

Figure 4 is an example of a fit to the Feb. 1998 data with one of the models. The geocoronal emission, also shown in the figure, is assumed to be the sum of two exponential at the two ends of the scan (large zenith angles), plus a linear background. The exact shape has a very small influence on the results. Figure 4 shows the derived relationship between $\Delta\phi$ and $v_{\rm He}$ and the interval found for $v_{\rm He}$. $v_{\rm He} = 24.5 \pm 2$ km s^{-1} is derived, independently of the other parameters. Figure 5 shows the same fit to the Feb. 1993 data, which gave the same result for $v_{\rm He}$.

4.4. Solar linewidth

The antisolar pointing of the LWS over one year sampled the He flow both upwind and downwind (though not a continuous sample). There is a pronounced minimum in the upwind flux (Fig. 6). This effect is due to the limited width of the solar line and is not a geocoronal effect. Atoms travelling towards the sun from upwind have large radial velocities, and they scatter the far red wing of the solar line. If the linewidth is too narrow, atoms are shifted out from the line. Thus, the narrower the line, the smaller the scattered upwind intensity. Due to the relative widths and velocities of the solar 58.4 nm line and the integrated He scattering distribution, the angular size of this feature is huge (~100°), so the LWS took ~100 days to scan across it from May to July, 1993, therefore more prone to short-timescale fluctuations in the illuminating/ionizing flux. The best fit solar Doppler linewidth using the LWS data over this time period is 35 km s^{-1}.

The 360° continuous scans performed in February 1993 have the advantage over the LWS data of including lines of sight near both the upwind and downwind direction, taken essentially concurrently. Figure 7 shows that the model intensity for the Feb. 1993 data has a pronounced minimum towards the upwind region. This effect is due to the limited width of the solar line and disappears for the high latitude lines-of-sight. Figure 7 shows three models for three different values of $\Delta w_{\rm D}$, including the best-fit model found to be

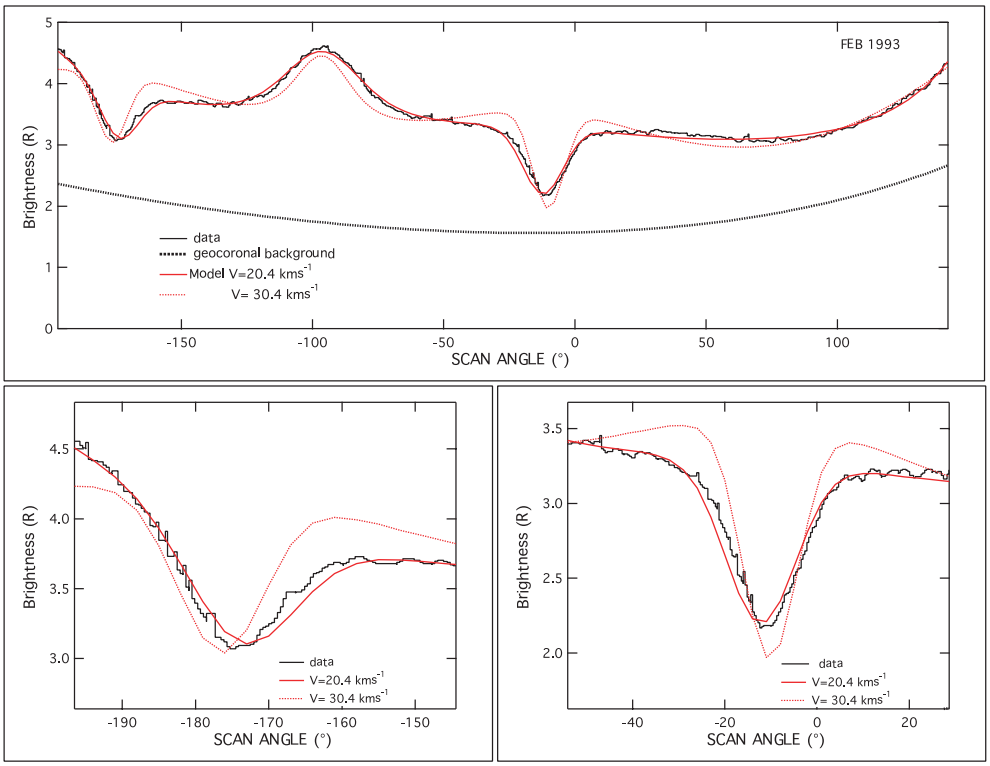

Fig. 5. Determination of the He flow velocity modulus with the Feb. 93 data.

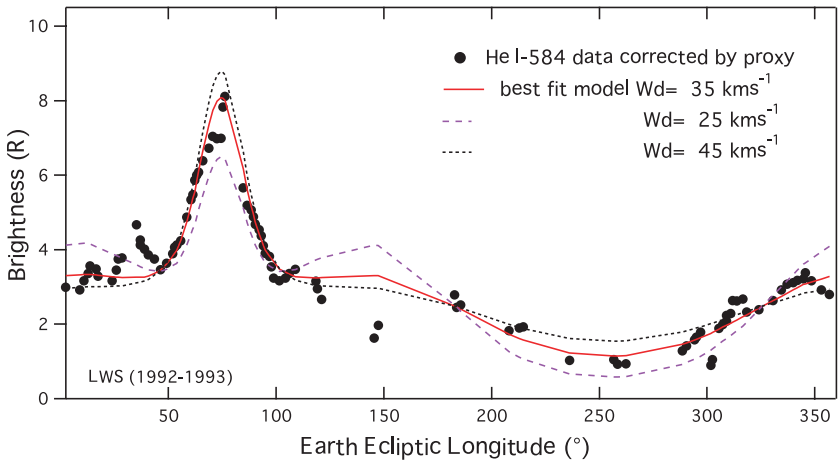

Fig. 6. Determination of the solar linewidth using the LWS antisolar data. Models are scaled at 50 and 100 deg longitude. Doppler widths above 45 km s^{-1} and below 25 km s^{-1} are precluded.

for $\Delta w_{\rm D} = 38 \pm 4$ km s^{-1}. This is in excellent agreement with the SUMER data mentioned above. Though this data has a higher signal to noise ratio compared to the LWS and the features are continuously sampled, it does suffer from the underlying geocoronal background, which we modeled with a linear slope and two exponential terms at satellite dawn and dusk.

4.5. Temperature

Once the kinematical parameters and the linewidth are determined, the temperature and the ionization rates can in principle be derived from the width and height of the emission from the focusing cone. However, these parameters are slightly interdependent. This is why we take advantage of the solar proxies and choose two different approaches. We first assume that the McMullin et al. ionization rate is precisely the actual value for the Oct.–Dec. 92–93 period corresponding to the LWS data in the downwind region, and for the Feb. 98 period, and we fit the temperature to both data sets. Figure 8 shows the resulting fit for the LWS. The derived temperature is $T = 6500$ K $\pm$ 2000 K for the for the 92–93 antisolar data, and $T = 9000$ K $\pm$ 1500 K for the Feb. 98 scan. The Feb. 93 scans give a best fit temperature of $T = 6000 \pm 1500$ K consistent with the contemporaneous LWS data.

The higher temperature derived for the Feb. 1998 data is a significant result, though its interpretation as an actual

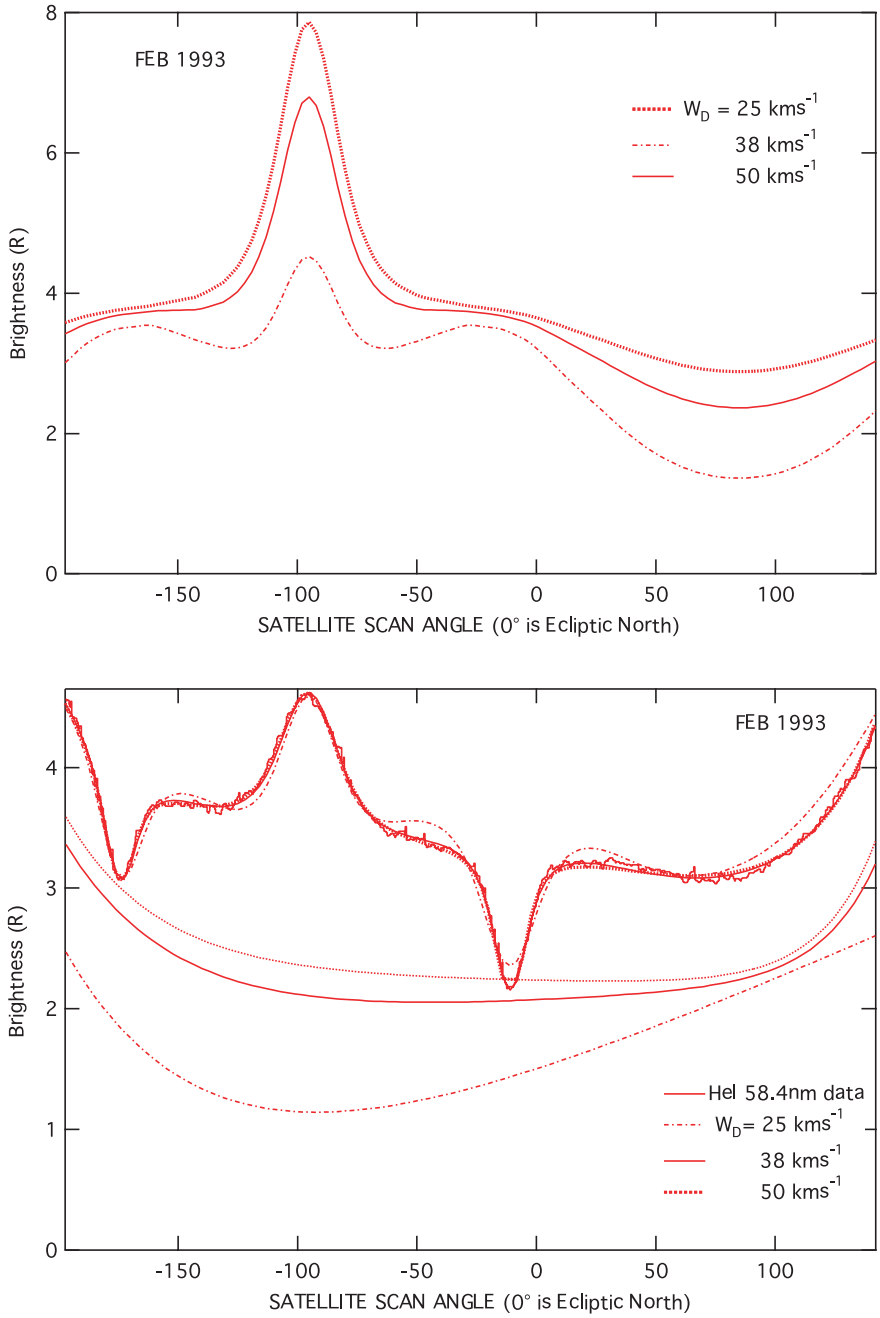

Fig. 7. Determination of the solar linewidth using the Feb. 93 scan. *Top*: models for the three Doppler widths: $\Delta w_{\rm D}$ = 25, 38 (best fit) and 50 km s^{-1}. The illuminating flux is 2.1×10^9 ph cm^{-2} s^{-1}, appropriate for the period of time. *Bottom*: models adjusted to the data for a free smoothly varying geocoronal contamination (see text). For small Doppler widths, it is not possible to fit correctly the center of the north absorption feature.

temperature shift is questionable. The downwind cone in 1998 is wider in latitude than the 1993 cone. In our model, only the temperature parameter can significantly widen this feature and is not constrained by other internal data. We believe this discrepancy might be caused by anisotropies in the illuminating/ionizing flux vs. ecliptic latitude, which are not included in our model. The 1998 data were taken right after solar minimum, where one would expect more latitudnal variation. Since the LWS sampled only the ecliptic plane, and the Feb. 1993 data was close to solar maximum, it is not surprising that they are more consistent with the particle derived temperature.

If we use the temperature derived by Witte et al. (2004) and vary the ionization rate (Fig. 9), we get derived values of $\nu_{\rm Total} = 0.95 \times 10^7$ s^{-1} consistent with the proxy estimates.

4.6. Density

Once the solar parameters, the flow velocity vector and temperature are adjusted, the measured intensity can be used to derive the neutral helium density, as a function of the solar intensity. For the antisolar 92–93 data, using the LWS spectrometer results and the solar 58.4 nm intensity derived from

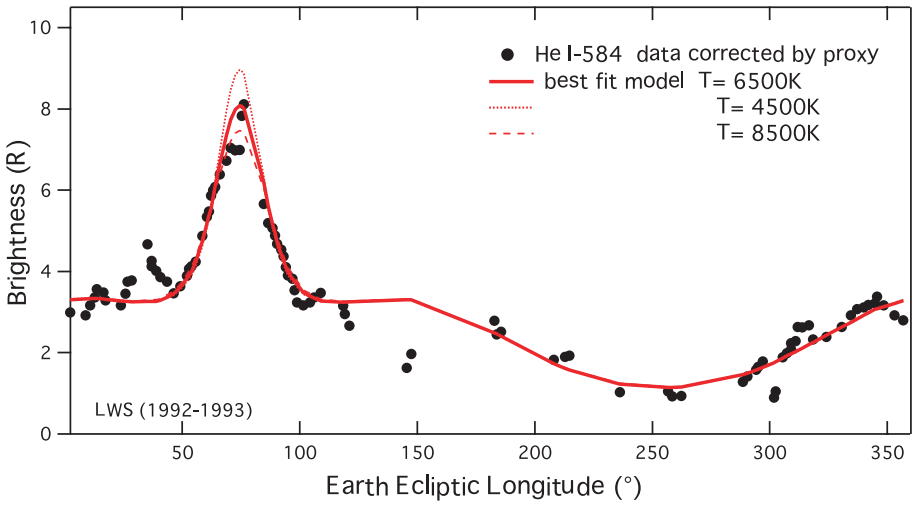

Fig. 8. Influence of the temperature. The solar ionization rate and the solar 58.4 nm line intensity are chosen according to the proxies. The best temperature in this case is between 4500 and 8500 K.

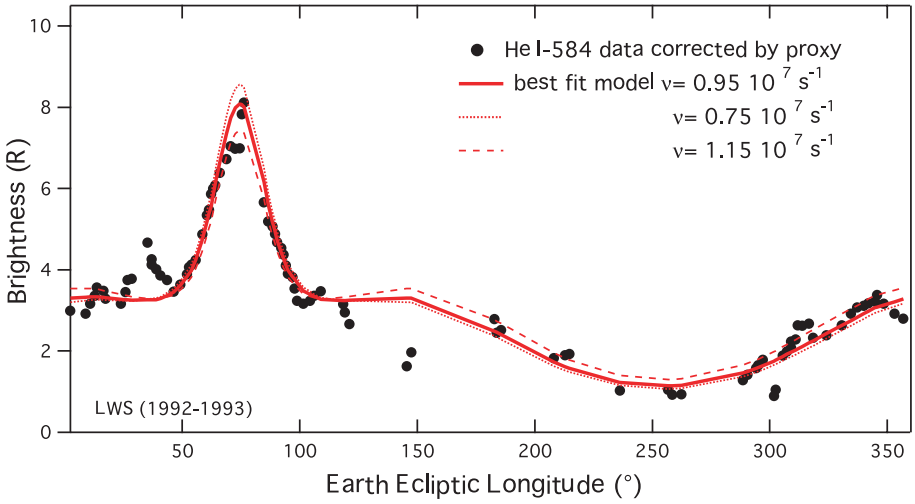

Fig. 9. Influence of the ionization rate.

the MgII-CDS proxi in 92−93, the resulting density $n_0 = 0.013 \pm 0.003$ cm^{-3}. This is in excellent agreement with the density derived from the in situ data.

The same method applied to the Feb. 98, Feb. 93 and 2000 Scanner data leads to a value $n_{\rm He} = 0.0075 \pm 0.003$ cm^{-3}, smaller by a factor of ≈1.75 than the LWS value. This discrepancy is troubling, as it calls in question the cross calibration of two instruments similarly calibrated with the same instrumentation before launch. The density is the only parameter discussed so far that depends on the knowledge of the absolute throughput to diffuse radiation of the instruments (effective area at 58.4 nm times the effective solid angle Ω). EUVE was designed to observe EUV point sources, and its response to point sources was calibrated in orbit using "standard" continuum stars like the hot white dwarf HZ43. The on-axis sensitivity to point sources did not change by more than a few percent over the life of the mission for both scanners and spectrometers (Sirk et al. 1997; Vallerga et al. 1998). The solid angle of the imaging photometers and the spectrometer collimators were never directly calibrated, though geometrical models and ray tracing of the vignetting functions give estimates that should be good to 10 percent. At this point, the relative factor of two discrepancy between the LWS and the ScC determination of absolute diffuse flux, and hence neutral helium density remains unexplained. This discrepancy does not have any impact on the quality of the other derived helium parameters, that depend on differential measurements and angular distributions of flux.

Another possibility is again the unmodelled anisotropy of the ionizing flux. The EUVE Scanners sampled the cone in a plane perpendicular to the ecliptic while the LWS sampled in the ecliptic plane, where more ionization might occur. Our models assumed isotropic ionization and the fact that the Scanners and LSW disagree on the normalizing density factor might indicate that this assumption is false.

5. October 2000 scans

As described above, the 5 scans done in October, 2000 sample the downwind cone at different radial distances from the

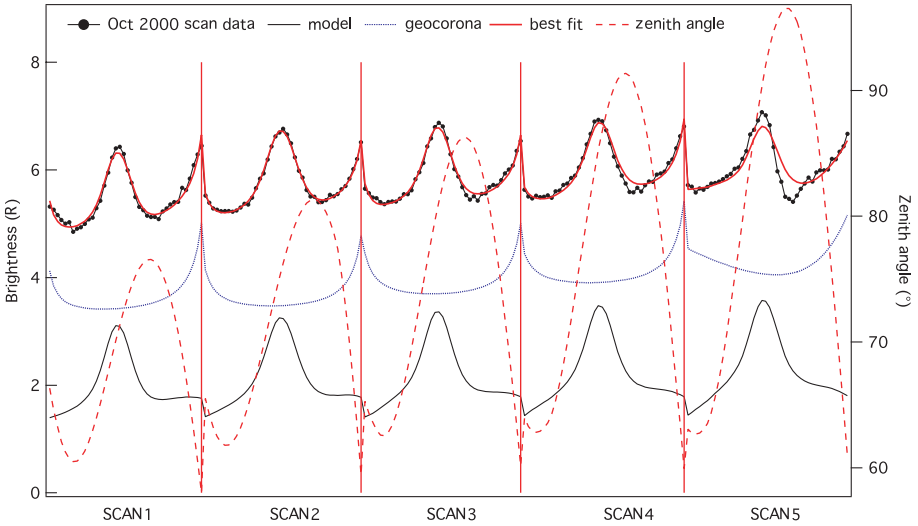

Fig. 10. Data from the 5 October, 2000 half-scans. Each of the 5 scans across the He cone intercept the cone at different solar radii, with the distance to the sun decreasing with scan number. The model adjusted to parameters found from our other data sets is found to fit reasonably well, with only the geocoronal background as a free parameter. The data do not fit at all when the line of sight is too low (local zenith angle above 85 degrees). Such that the LOS intersects deep into the Earth's atmosphere.

sun. This geometry is significantly different from the February data scans that we felt it would be a good test to see if the parameters derived from the extensive fitting of the previous data could predict directly the Oct. 2000 data without any free parameters except allowing the geocoronal background to change and using the appropriate proxies for the solar illumination and ionizing parameters. Figure 10 shows the data and the model for the 5 scans which progress closer to the Sun at each scan. Unfortunately, the Earth's atmosphere got in the way for the closest scans to the Sun, but for the others, the model vs. data comparison is quite good, giving us confidence that the model works in arbitrary lines of sight and that the He parameters are well known.

6. Conclusions

Using solar EUV backscattered photons at 58.4 nm measured with EUVE and a fully kinetic model of the helium flow distribution, we have been able to precisely measure the bulk flow velocity vector of the local interstellar neutral helium, consistent with the velocity measurements of particle instruments. Of slightly less accuracy are the helium temperature and density measurements, as they depend on the absolute calibration of the diffuse response of the instruments aboard EUVE, which was never designed for this purpose. However, the results obtained using our ground calibrations are consistent with the other measurements, and the combination of our analysis with the complementary particle missions makes for a stronger overall result.

Remote sensing of the EUV backscatter radiation is a powerful tool to characterize the parameters of the scattering gas and the illuminating source (the Sun). Unfortunately, this was realized too late to be optimally used by EUVE, as resources and time were directed at the end of the mission to its Guest Observer program. However, we estimate that more than 50% of the photons detected by EUVE are 58.4 nm and the data set spans an almost complete solar cycle. Now that proxies and good models exist, mining the EUVE archive could investigate the short term variability of the solar parameters and improve the velocity parameters with better modeling of the geocoronal background.

Acknowledgements. The authors wish to thank Dr. Roger Malina, the former Director of the Center for EUV Astrophyics who graciously provided Director's discretionary time to observe the interplanetary helium. This work was initiated and partly carried out with support from the International Space Science Institute in the framework of an International Team entitled "Physical parameters of the LISM through coordinated observations of the gravitational focusing cone at 1 AU". Some of this effort was supported by the NASA contract NAS5-29298.

References

Ajello, J. M. 1978, ApJ, 222, 1068
Bertin, P., Lallement, R., Ferlet, R., & Vidal-Madjar, A. 1993, J. Geophys. Res., 98, 15193
Bowyer, S., & Malina, R. F. 1991, Extreme Ultraviolet Astronomy, 397
Costa, J., Lallement, R., Quémerais, E., et al. 1999, A&A, 349, 660
Dalaudier, F., Bertaux, J. L., Kurt, V. G., & Mironova, E. N. 1984, A&A, 134, 171
Flynn, B., Vallerga, J., Dalaudier, F., & Gladstone, G. R. 1998, JGR, 103, 6483
Judge, D. L., Ogawa, H. S., McMullin, D. R., Gangopadhyay, P., & Pap, J. M. 2002, Adv. Space Res., 29, 1963
Lallement, R. 1999, Solar Wind Conference, 205
Lallement, R. 2002, in The Century in Space, ed. Bleeker, Geiss, Huber (Kluwer Ac. Publ.)
Lallement, R., & Bertin, P. 1992, A&A, 266, 479
Lallement, R., Raymond, J., Bertaux, J. L., et al. 2004a, A&A, 426, 867
Lallement, R., Raymond, J. C., Vallerga, J., et al. 2004b, A&A, 426, 875

Lamy, P., Llebaria, A., & Quemerais, E. 2002, Adv. Space Res., 29, 373
Lang, J., Thompson, W. T., Pike, C. D., Kent, B. J., & Foley, C. R. 2002, in The radiometric calibration of SOHO, ISSI Scientific Report, ed. A. Pauluhn, M. Huber, & R. Von Steiger
Lemaire, P. 2003, private communication
McMullin, D. R., Judge, D. L., Phillips, E., et al. 2002, SOHO 11 Symp., ESA SP-508
McMullin, D., Bzowski, M., Mbius, E., et al. 2004, A&A, 426, 885
Mobius, E., Rucinski, D., Isenberg, P. A., et al. 1995, Adv. Space Res., 16, 357
Rucinski, D., & Fahr, H. J. 1989, A&A, 224, 290
Rucinski, R., Cummings, A. C., Gloeckler, G., et al. 1996, Space Sci. Rev., 78, 73
Sirk, M. M., Vallerga, J. V., Finley, D. S., Jelinsky, P., & Malina, R. F. 1997, ApJS, 110, 347
Vallerga, J. V., Roberts, B., Dupuis, J., & Jelinsky, P. N. 1998, Proc. SPIE, 3356, 1001
Vallerga, J. 1996, Space Sci. Rev., 78, 277
Weller, C. S., & Meier, R. R. 1981, ApJ, 246, 386
Wilhelm, K. 2003, private communication
Witte, M., Rosenbauer, H., Banaszkiewicz, M., & Fahr, H. 1993, Space Res., 13, 121
Witte, M., Banaszkiewicz, M., & Rosenbauer, H. 1996, Space Sci. Rev., 78, 289
Witte, M. 2004, A&A, 426, 835